Astron. Astrophys. 332, 703–713 (1998)

ASTRONOMY
AND
ASTROPHYSICS

Monte Carlo simulations at very high optical depth: non-LTE transfer in H_2O in the protostellar object B 335

Daniel Hartstein and René Liseau

Stockholm Observatory, S-133 36 Saltsjöbaden, Sweden (daniel@astro.su.se; rene@astro.su.se)

Received 12 March 1997 / Accepted 4 December 1997

Abstract. We present a formulation of the Monte Carlo method which should be capable of treating radiative transfer problems even at very high optical depths ($\tau \gg 10^4$) and apply this tool to predict rotational H_2O line spectra for the protostellar object B 335 for future observational tests with space borne facilities. The physical model of the source is based on published observations in lines of CS, for which we obtain model results which are in agreement with previous computations. We apply our model also to line profiles of CO isotopomers observed at high spatial resolution and derive the total CO cooling rate for B 335. From the comparison with the derived H_2O cooling rates, we are led to conclude, quite generally, that H_2O is probably not the major coolant of low-mass protostellar collapse.

Key words: ISM: clouds – ISM: individual objects: B 335 – ISM: molecules – ISM: kinematics and dynamics – stars: formation – methods: numerical

1. Introduction

Recently, a few objects have been found which, on the basis of high resolution molecular line observations, appear to be protostars undergoing gravitational collapse (Gregersen et al. 1997). The hitherto best studied and most convincing case is that of B 335, an isolated Bok globule at the adopted distance of 250 pc ($130 \lesssim d \lesssim 400$ pc) and of age, perhaps, 60 Myr (Frerking et al. 1987). The central far infrared object is of low luminosity, 2 to 3 $L_\odot$ (Keene et al. 1983, Chandler et al. 1990), and drives a bipolar outflow lying nearly in the plane of the sky (Langer et al. 1986; Hirano et al. 1988, 1992; Cabrit et al. 1988; Moriarty-Schieven & Snell 1989).

Zhou et al. (1993) observed this source in several rotational transitions of carbonsulfide, CS, and of formaldehyde, H_2CO, and found line profiles with asymmetries between the red and blue emission peaks indicative of mass infall. Zhou et al. (1993, 1994; hereafter Z93, Z94) obtained good fits to the observed profiles using a spherically symmetric inside-out collapse model (see Fig. 1). The velocity field and the density structure are in this case given directly by the theory (Shu 1977), whereas the kinetic gas temperature was determined from observations of the associated dust, assuming equilibration of the gas and dust temperatures in the source (Zhou et al. 1990; hereafter Z90). An advantage with the Shu theory from the modeling point of view is that only two parameters, the infall radius, $R_{\rm inf}$, and the 'effective' (including non-thermal random motions) sound speed, $a_{\rm eff}$, provide a complete description of the density distribution and the velocity field.

In these models, the LVG method (Large Velocity Gradient) was exploited to treat the radiative transfer. However, the LVG assumption is not consistent with the velocity field actually predicted by the Shu theory (Fig. 1). One of the known techniques, by means of which the radiative transfer for arbitrary velocity fields is treated correctly, is the *Monte Carlo* method (hereafter, MCM; for a recent detailed accountance of history and application: see Juvela 1997). Using MCM, Choi et al. (1995) have recently re-calculated the line profiles for B 335 resulting from the Shu model. In addition, they also used more recent CS collisional rates. Compared to the work by Zhou et al., their best fit model gave somewhat different parameters.

Molecular lines are an important tool for the study of stellar formation. However, some molecules, which are believed to be very important for the physics and chemistry of collapsing cores, are not readily observable from the ground. This is particularly true for O_2 and H_2O, the lines of which are effectively blocked by the Earth's atmosphere. Thanks to new satellite borne far infrared and sub-millimetre facilities with high spectral resolving powers, such as ODIN and FIRST, this is about to change. Of particular interest are the spectral lines of water vapour, H_2O, spanning a large range in physical excitation conditions. These lines are believed to provide the major cooling during the collapse phase (e.g. Hollenbach et al. 1995, Ceccarelli et al. 1996, and references therein). Since many of the water transitions could be *very* opaque ($\tau \gg 10^4$), standard MCM radiation transfer techniques are not suitable to model these lines, owing to the method's intrinsic incapability to handle large optical depths.

To overcome this problem we have developed a modified Monte Carlo scheme, incorporating the 'core saturation'

Send offprint requests to: R. Liseau

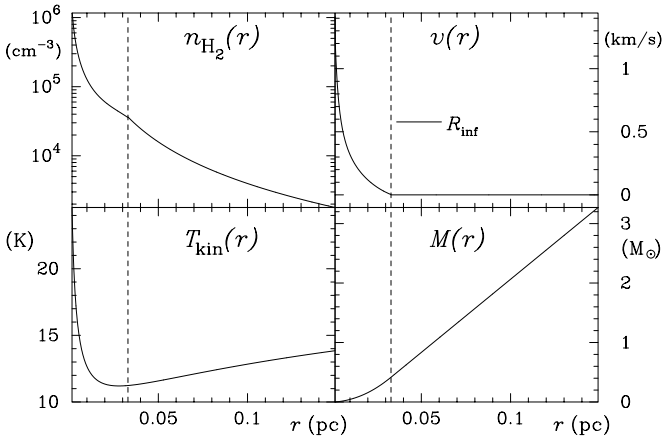

Fig. 1. Radial profiles of the density, $n(H_2)$, velocity, v, temperature, T, and cumulative cloud mass, M, of the inside-out collapse in B 335 according to our best fit model (see: Sect. 3.1). The infall radius at time t, $R_{inf} = a\,t$, is indicated, where a is the velocity of the 'expansion wave' (Shu 1977)

method. In this paper, we present rotational line spectra computed for H_2O assuming the Shu infall model for B 335. These model spectra will be compared with observation, hopefully, in the near future. From this comparison, we ought to be able to determine the total H_2O abundance, including the ortho-to-para ratio ($o:p$), in B 335 (and in other sources) and, hence, the cooling efficiency of the water lines. In addition, observation of the profiles of various lines should enable us to learn about the dynamics of the infall candidates. For this purpose, the best fit MCM model was selected on the basis of the CS observations by Z93, such that the CS results were used to determine the physical parameters of the B 335 infalling envelope, which were then applied to the H_2O modeling. In addition, we have also calculated isotopic CO spectra for the comparison with existing observations and, finally, studied some modified infall scenarios to explore to what extent they could equally well or better explain the CS observations.

The organization of this paper is as follows: in Sect. 2, we shortly describe the numerical method, including our implementation of the (line) core saturation method and of the dust continuum transfer, whereas the more detailed discussion is deferred to the Appendices A and B at the end of the paper. We apply the method in Sect. 3 to model existing observations of B 335 in CS and in isotopic CO and to predict H_2O spectra for future observational tests. These results are discussed in Sect. 4, where we examine the uniqueness of the Shu model fits and determine the CO and H_2O cooling functions for the B 335 infall case. At the end of that section, we discuss the advantages and limitations of our modeling approach and point shortly towards possible future improvements. Finally, in Sect. 5, we briefly summarize our main conclusions from this work.

2. The numerical method

2.1. Monte Carlo simulations of radiative transfer

To treat the radiative transfer we built on a Monte Carlo code originally developed by Bernes (1979) and improved by Bergman (1985). The theoretical basis of this code is described in Appendix A. Here, a shorter summary is given.

The basic idea of MCM is to simulate the radiation transport. This is accomplished by sending out model photons in random directions and at random frequencies, each with a weight W in proportion to the number of real photons thought to be emitted by the source. In the present case, the model cloud is composed of a series of concentric spherical shells, each having its own values of the local physical parameters such as the volume density, $n(H_2)$, the gas and dust temperatures, T_{gas} and T_{dust} respectively, the molecular abundance, X_{mol}, and the microturbulence, ξ_{turb}. The model photons are followed across the cloud, causing excitations and de-excitations along their paths, which alter the energy level populations of the molecules in the different shells. In addition to photons from the molecular gas in the source, photons which represent background radiation, dust radiation and radiation from a central black body (stellar source) may also be emitted. After adjustment of the level populations, new model photons are sent out, and the process is repeated. This iterative scheme is continued either for a fixed number of iterations or until some pre-specified criterion for convergence is fulfilled.

From the final populations in the different radial shells, the flux density to be observed at any frequency is calculated by computing the frequency dependent specific intensity along separate lines of sight, and then convolving this intensity map with the diffraction pattern of a telescope (the 'telescope beam'), which here for simplicity is assumed to be represented by a Gaussian. This convolution is a numerical integration directly in 'image-space', i.e. not in 'Fourier-space'. To comply with chopped observations, the contribution by the cosmic microwave background radiation has been subtracted from the model spectra.

The great advantage of MCM, compared to other methods commonly in use (e.g. LVG), is that it allows a consistent treatment of the radiative transfer for arbitrary velocity fields and density distributions. For reasons becoming apparent below, we here limit ourselves to a spherically symmetric geometry, but the generalization to arbitrary geometries is relatively straightforward (e.g., see: Juvela 1997). With presently available computing facilities, such generalization is however not yet feasible, if we wish to keep with the high spatial and frequency resolution aimed at in this paper.

A major disadvantage of MCM is the fact that, in its original formulation, the method is not well adapted to cope with very high optical depths, such as can be found in, e.g., spectral resonance lines. Since we here are interested in the computation of H_2O line profiles, this property presented initially a problem. In physical models of interest, many of the water lines are expected to be very optically thick (τ of the order of 10^2 to 10^5). To overcome this problem we have modified the original Monte

Carlo 'recipe' by incorporating a method known as 'the core saturation method'.

2.2. MCM and very high optical depths: the core saturation method

In standard Monte Carlo transfer simulations, convergence will become extremely slow once optical depths become very large, because each iteration can propagate the necessary corrections only with a step $\Delta\tau$ of order unity. This is exactly the same problem as encountered in classical Λ-iteration (see, e.g., Mihalas 1978). To make it possible to treat the radiative transfer in the water lines we have implemented into the MCM the *core saturation method*, originally developed by Rybicki (1972). This method is a way of analytically eliminating from the calculations the line core photons assuming that these do not contribute much to the transfer process. In order to specify those parts of the spectral line belonging to the core and to the wings respectively an adjustable parameter γ is introduced, which represents the optical depth separating the core from the wings. In its basic formulation, the method is not exact. We introduce, therefore, a correction procedure which represents an *exact analytical solution*, implying that also the MCM results for converged calculations should be exact, limited in accuracy only by the MCM noise. The implementation of the core saturation method together with our correction procedure into the Monte Carlo scheme is described in Appendix B.

2.3. Continuum radiation from associated dust

The code was extended to take into account also the dust continuum. Scattering was jugded to be of little importance, since typical particle sizes are supposedly much smaller than characteristic wavelengths of the far infrared/submm radiation. Hence, we considered only the absorption and the emission processes for the dust particles.

For the absorption, the dust optical depth is calculated as $\mathrm{d}\tau_\nu = \kappa_\nu \rho \,\mathrm{d}z$ and added to the line optical depth at the frequency ν. Here, ρ is the total mass density and κ_ν is the mass absorption coefficient of the dust, expressed on a total mass scale, i.e. a constant gas-to-dust mass ratio has been included. Z90 found that the dust opacity of Mathis et al. (1983) best reproduced their observations and, accordingly, we have used this dust model in our calculations.

To treat the emission we assume that the dust particles emit a thermal spectrum at $T = T_{\rm dust}$. By virtue of Kirchhoff's law, the number of photons emitted per second by the dust can be written as $(4\pi/h\,\nu)\,\kappa_\nu\,\rho\,V_m\,B_\nu(T_{\rm dust})\,\Delta\nu$, where h is Planck's constant and V_m is the volume of shell m. Because κ_ν varies only slowly with frequency, these 'dust photons' are distributed uniformly over the passband $\Delta\nu$ and are sent out together with the other model photons.

2.4. Performance and testings of the code

The MCM is a numerical *simulation* and, as such, difficult to verify in its extreme applications. If *exact* solutions or schemes existed, these would of course be preferable and the use of simulations be superfluous. The method can be fully tested, therefore, only within a limited range of the parameter space and the results outside these boundaries can be expected to be valid by induction. The final verification will have to rely, however, on comparisons with experimental data.

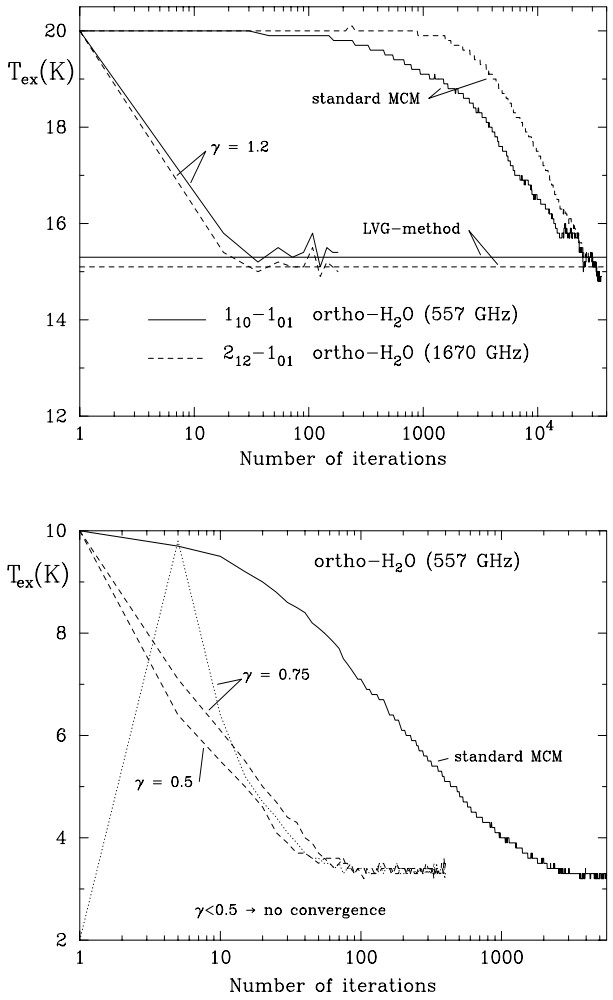

Fig. 2. Performance of *standard*-MCM and MCM with *core saturation* implemented. The number of iterations are shown along the abscissa and along the ordinate, the excitation temperature, $T_{\rm ex}$. The iterations have converged, once $T_{\rm ex}$ fluctuates about a constant value. **Upper:** The LVG model case (for details, see the text). The LVG excitation temperatures for the displayed transitions in ortho-H_2O, viz. $1_{10} - 1_{01}$ and $2_{12} - 1_{01}$, are shown by the horizontal lines. Opacities in both lines are very high ($\tau_0 \gtrsim 10^4$). Whereas the calculations with core saturation converged rapidly, those of the standard MCM had not converged after about 35 000 iterations. **Lower:** The B 335 model (see: Sects. 3.1 and 3.3) at relatively high line opacity in the 557 GHz groundstate transition of ortho-H_2O ($\tau_0 \approx 1\,500$). Two values of the core saturation parameter γ are indicated. A test case, for which the calculations were started from 'below' ($T = 2$ K), is also shown. The calculations without core saturation needed 5 000 iterations for convergence, whereas those with core saturation had all converged after less than ~ 200 iterations

2.4.1. Tests by comparison with other methods

The correctness of the implemented core saturation algorithm was tested in two ways, viz. by comparing (with highly time consuming runs) with the original code without core saturation (up to optical depths $\tau \sim 1\,500$) on one hand, and on the other, by comparing with model constructions for which the LVG approximation is valid and which were run up to $\tau \gtrsim 10^4$. As expected, convergence of the MCM with core saturation is found to become much faster (see Fig. 2). The stability (or 'robustness') of the convergence was tested by drastically altering the start values (Fig. 2).

To test the code for cases with very high optical depths we made use of a homogeneous model with a constant velocity gradient, in which case the radiative transfer could be correctly treated with the LVG technique. Specifically, these tests were made for models with $n(H_2) = 10^3$ and 10^5 cm^{-3}, respectively, and where the water abundance was chosen such that the optical depths in the two groundstate lines of ortho-H_2O (557 GHz and 179.5 μm) exceeded 10^4. In the upper panel of Fig. 2 it is demonstrated that our modified MCM code leads to nearly instantaneous (about 20 iterations) convergence towards the excitation temperatures found from the LVG run, whereas the standard MCM had not converged even after some 35 000 iterations.

2.4.2. Choice of core parameter γ

Acceptable γ values have to guarantee computational convergence and the best choice is somewhat a matter of trial-and-error, but normally not very critical. However, if γ is chosen too small, convergence will become problematic, because the core saturation approximation becomes increasingly less exact with decreasing γ. But there is also the additional problem that, if a large relative number of the model photons happen to be sent out in the core and are thus 'inactive', the noise (random fluctuations) inherent in MCM increases. This has the effect that the resultant level populations either simply diverge, or in 'less severe' cases, the noise may grow too large to allow the populations to settle at their correct values (see Fig. 2). This problem can be reduced by increasing the number of model photons or by increasing γ. If the optical depth is increased, the number of photons necessary to arrive at a stable convergence increases too, because with growing opacity a larger percentage of the model photons will be sent out in the core and, thus, not contribute to the iterative process. In most model cases presented below, we applied values of $\gamma \sim 1$.

2.4.3. Numerical accuracy and computational speed

The accuracy of the presented computations is limited by the noise inherent in MCM, i.e. independent of whether the core saturation routine is 'on' or 'off'. This numerical 'photon noise' is inversely proportional roughly to the square root of the number of model photons. The noise level can be brought down, therefore, by increasing the number of model photons at the cost of the corresponding increase in computing time, t. However, low noise is no guarantee for convergence, as is exemplified in the upper panel of Fig. 2. There, the standard MCM calculation never converged, in spite of the low noise level.

The computing time depends on the number of model photons and the number of iterations, viz. $t \propto N_{\rm phot} \times N_{\rm iter}$. Because of the γ-dependence (see Sect. 2.4.2), $N_{\rm phot}$ needed for convergence is difficult to quantify analytically for the core saturation method and, furthermore, will vary from case to case. To give an example, for the case of Fig. 2 (upper panel) the relative gain in time with core saturation was a factor $\gtrsim 10$, viz. $(9\,10^4 \times 20/600 \times 3.5\,10^4)^{-1} = 1/0.086$. However, considering the fact that the standard method did not even converge would imply that the gain can actually become infinite.

Although there is no obvious theoretical limit to the application of the code ($\tau_0 \rightarrow \infty$), available computing power will in practice constrain also the usefulness of the core saturation method. The convergence will become problematic, because eventually the relative number of wing photons will become too small. According to our present experience, the core saturation MCM works satisfactorily up to optical depths $\lesssim 10^5$.

3. Results

3.1. CS lines: determining the physical model

Using our Monte Carlo code we have computed line profiles of rotational CS transitions which result from Shu-type infall models for the purpose of comparison with other model calculations and with the observations of B 335 by Z93. The nine lowest rotational energy levels of the CS molecule were considered. The collision rates, which are identical to those used by Choi et al. (1995), were taken from Turner et al. (1992). These rates were actually computed for collisions of CS with He and we applied a first order correction ($\times 1.4$) to obtain the rates for collisions with H_2. In our calculations, collisions with both He and H_2 are considered, contributing to the total rates, with the helium abundance $X_{\rm He} = 0.2$. The lowest temperature, for which these recent collisional rate coefficients are tabulated, is 20 K. For B 335, extrapolating downwards to ~ 10 K is required. From comparison with earlier data, we estimate that the error introduced by this extrapolation should not exceed 20%.

The same constant value of the microturbulence, viz. $\xi_{\rm turb} = 0.12$ km s^{-1}, was used by us and in the previous computations by Z90, Z93, Z94 and by Choi et al. (1995) and, of course, we adopted also the same temperature structure, determined from the dust observations by Z90. Our model cloud consisted of 30 shells with outer radii from $1.1\,10^{15}$ cm to $4.6\,10^{17}$ cm (74 AU to $31\,10^3$ AU), corresponding to $0\farcs3$ to $2'$ at the distance of 250 pc. Tests confirmed that increasing the number of shells or extending the model cloud beyond the stated limits had no significant effects on the results.

For the comparison with observation, we recall the comment by Z93 that the observed position of the absorption dips for the different lines does not match completely. As possible explanations these authors offered inaccurate settings of the local oscillator or the use of inaccurate rest frequencies. We have

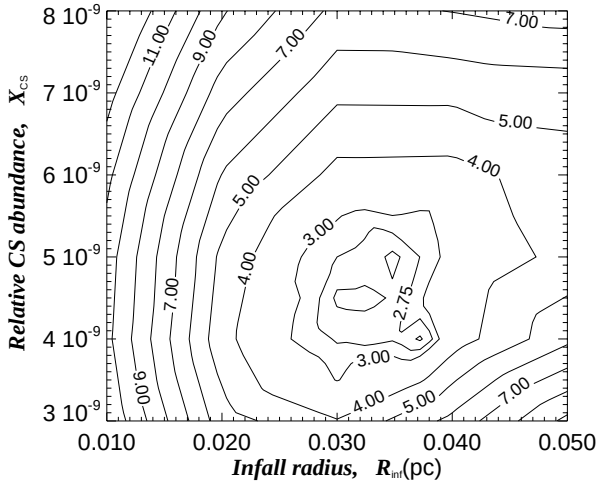

Fig. 3. The contours show the reduced χ^2 for the CS abundance (y-axis) and the infall radius (x-axis) for the Shu-type infall model of B 335 and the CS line observations by Z93. min χ^2 is found near $X_{\rm CS} \sim 4.5\,10^{-9}$ and $R_{\rm inf} \sim 0.033$ pc

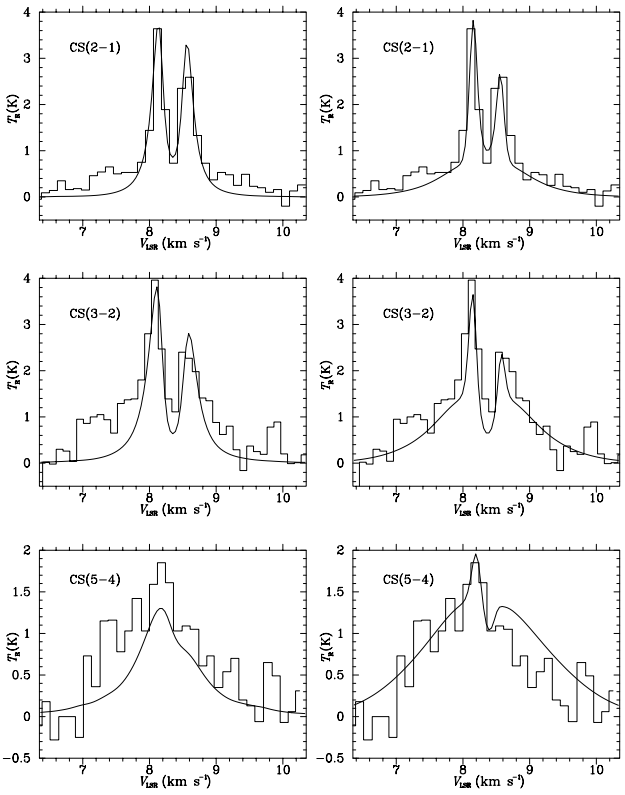

Fig. 4. Left panels: The CS lines, predicted by our best fit model of Shu-type infall in B 335 ($R_{\rm inf}$ = 0.0325 pc, $X_{\rm CS}$ = 4.5 10^{-9}, $\xi_{\rm turb}$ = 0.12 km s^{-1}), superposed onto the observations by Z93 shown as histogrammes. **Right panels:** The observations by Z93 are compared to a power-law model with variable microturbulence, $\xi_{\rm turb}(r)$ (for details, see Sect. 4.1)

simply shifted, therefore, each computed line in radial velocity until it coincided with the observed profile. Keeping the position of the absorption dip fixed at $v_{\rm LSR} = 8.35$ km s^{-1}, these shifts were -0.15 km s^{-1} for CS (2-1), (5-4) and +0.05 km s^{-1} for (3-2).

The parameter space of the model was explored between $R_{\rm inf} = 0.01$ pc and 0.05 pc, and from $X_{\rm CS} = 3\,10^{-9}$ to $8\,10^{-9}$, respectively. To evaluate the goodness of the fit between the model and the observations, we followed Choi et al. (1995) and calculated, in the velocity interval 7.65 to 9.05 km s^{-1}, the reduced $\chi^2 = (1/N)\sum[(T_{\rm model} - T_{\rm obs})/\Delta T_{\rm obs}]^2$, where T and $\Delta T_{\rm obs}$ are the line radiation temperature and rms-noise in Kelvin, respectively, and N is the number of spectral points (Fig. 3). Our results agree well with those of Choi et al. (1995). Our *best fit* to the CS observations was achieved, formally, for $R_{\rm inf}$ = 0.0325 pc (27″ at 250 pc) and X(CS) = 4.5 10^{-9}. The resulting CS line profiles from this model are shown together with the observed profiles on the left hand side of Fig. 4. This model provided the basis for the computations discussed in the following sections.

3.2. Isotopic CO lines: infall profiles?

Chandler & Sargent (1993) have observed B 335 in the (1-0) lines of ^{13}CO and C^{18}O at high spatial resolution. In the aperture synthesis of these interferometer observations, an artificial beam of 5.″6 × 4.″8 was exploited and the presented spectra were the result of averaging over a 5″ × 5″ box about the map centre. The observed ^{13}CO line displays an asymmetric profile, with a red shoulder-like wing, whereas the C^{18}O profile appears nearly symmetric. Chandler & Sargent interpreted these observations to indicate the presence of mass infall, assuming the C^{18}O emission to be optically thin.

For the comparison with these observations we have computed spectra of isotopic CO for our best fit CS model. Collisional rates are available for collisions with both He (Green & Chapman 1978) and with ortho- and para-H_2 (Flower & Launay 1985). Other molecular data were taken from Chakerian & Tipping (1983) and 12 energy levels were included. The ortho-to-para ratio, $o:p$, for H_2 was assumed to be 3 : 1. However, regarding the modeling of the (1-0) line of the CO isotopomers, we find that it is always thermalized throughout the cloud, and this ratio turned out, therefore, to have no effects on the results.

We have attempted to reproduce the procedure of Chandler & Sargent of generating the averaged spectra towards B 335 in the following way: assuming a Gaussian beam with FWHM = 5″ we simulated an observation of a 9 point map (5″ × 5″) and then averaged the results. Our source model of B 335 cannot fully reproduce the observed ^{13}CO and C^{18}O lines (Fig. 5). Whereas the model spectra grossly have the observed shapes, the computed flux densities are about twice those observed and, for ^{13}CO, the theoretical peak-to-shoulder ratio appears too small. For the model of the CS observations, we were unable to produce a ^{13}CO profile, which had *both* the correct flux density *and* an asymmetric profile of the shoulder-type observed. It is thus possible that the interferometer observations were missing some appreciable fraction of the flux from the relatively extended ^{13}CO source.

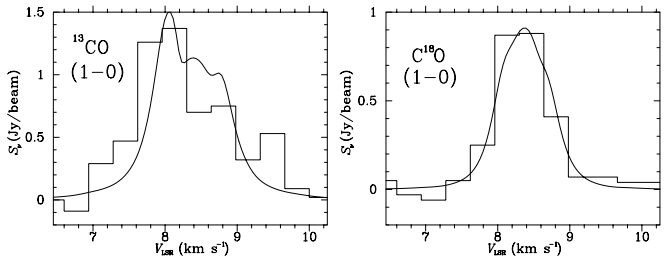

Fig. 5. Left: The ^{13}CO (1-0) line profile of the best fit CS model is shown superposed onto the interferometer observations by Chandler & Sargent (1993), displayed in histogram form. The derived ^{13}CO abundance is $X(^{13}\mathrm{CO}) = 5\,10^{-6}$ and the theoretical profile has been scaled by the factor of 0.5 (see text). **Right:** The C^{18}O (1-0) line profile ($\times$0.5) of the model compared with the observed line shown as histogram

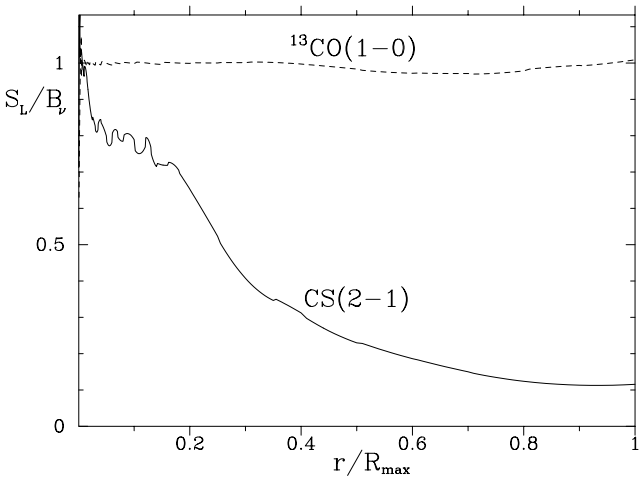

Fig. 6. The normalized line source functions for ^{13}CO (1-0) and CS (2-1) versus radial distance for the best fit CS model

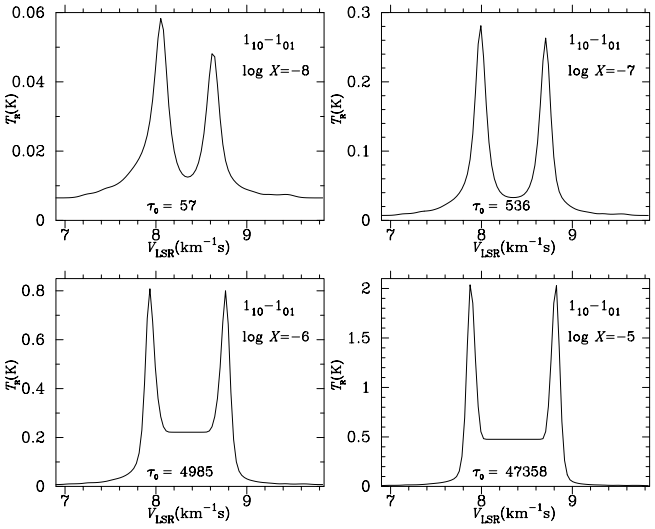

Fig. 7. B 335 in the ground state transition of ortho-H_2O at 557 GHz, ($1_{10} - 1_{01}$), as seen with the telescope aboard ODIN, to be launched into space in 1998. Indicated is the total (ortho + para) water vapour abundance and spectra are shown for the range from $X(H_2O) = 10^{-8}$ to 10^{-5} and $o:p = 3{:}1$ is assumed for both H_2 and H_2O. Also displayed in each panel is the line centre optical depth, τ_0. The apparent decrease of the blue-red asymmetry with increasing line opacity is artificially caused by the fix telescope beam ($2'$), since this emission becomes increasingly more compact

In order to produce the red shoulder of the ^{13}CO profile the molecular abundance relative to H_2 has to be greater than $2\,10^{-6}$. For the interstellar ^{12}CO abundance of about 10^{-4}, this result indicates that the average ^{12}CO/^{13}CO ratio in B 335 would be less than 50. From the profile fitting, our best estimate of the ^{13}CO abundance is $X(^{13}\mathrm{CO}) = 5\,10^{-6}$, yielding ^{12}CO/^{13}CO as low as about 20, which could indicate efficient/long-time mixing of the core gas with the photochemically processed surface layers. Further increase of $X(^{13}\mathrm{CO})$ has only marginal effects on the resulting line profile, but such high values can be excluded on the basis of the implied too small isotope ratios. The observed C^{18}O (1-0) line lacks distinctive features such as a well developed, characteristic shoulder, which makes the comparison with model results more ambiguous. The theoretical profile, shown in Fig. 5, is slightly red-asymmetric. This shape is also marginally exhibited by the observations, the velocity resolution of which is too low to be conclusive, however. The theoretical profile has been scaled by the factor of 0.5 (see above), being compatible with a C^{18}O abundance of about $X(\mathrm{C}^{18}\mathrm{O}) = 5\,10^{-7}$ and suggestive of the nearly normal ratio ^{13}CO/C^{18}O ~ 10.

Observations of ^{13}CO at spatial resolution comparable to that of the CS data of Sect. 3.1 do not exhibit profiles with asymmetries characteristic of infall (Menten et al. 1989). This is in agreement with our model calculations and can be understood in the following way: Since the ^{13}CO (1-0) transition is thermalized throughout the cloud and thus insensitive to the density gradient, the gradient in excitation temperature becomes much smaller than for the subthermally excited CS transitions (see: Fig. 6). Therefore, the ^{13}CO emission is centrally less condensed than the CS emission. Hence, the contrast of the ^{13}CO emission from the central regions, where velocities are large, compared to that from regions further out is lower than that of the CS emission. This will have the following consequences: (1) Compared to low-J CS observations, much higher spatial resolution is needed to detect signs of infall in the ^{13}CO (1-0) spectrum, and (2) the central dip in ^{13}CO will become smaller or, as in the actual case, disappear altogether.

3.3. H_2O line spectra: the ortho-to-para ratio

As for the CO lines in the previous section, we applied our best fit CS model of B 335 to calculate ortho- and para-water line spectra for this source with the total H_2O abundance as a free parameter. Spectra were computed in the range $X(H_2O) = 10^{-8}$ to 10^{-5} and, as before, the abundance was assumed to be constant throughout the model cloud. For each of the ortho-

and para-branches, the 8 lowest rotational energy levels were included with Einstein A-coefficients from Chandra et al. (1984) and with collisional rates from Phillips et al. (1996). As for CO in Sect. 3.2, rates are available for collisions both with H_2 and with He, and the ortho-H_2 rates differ from those for para-H_2. The total H_2O - H_2 collisional rate will depend, therefore, on the $o:p$-ratio of H_2.

Molecular hydrogen is created in the high temperature ratio $o:p = 3:1$, i.e. in the ratio of the statistical weights of the nuclear spins. However, at dense core temperatures, $T < 30$ K, this value could be much smaller. Compared to the presumptive lifetime of the cloud, the lowering of $o:p$ could be relatively fast, occurring on timescales of only about 10^6 yr (Flower & Watt 1984; Willacy et al. 1993). For instance, in B 335, Minh et al. (1995) have determined $o:p \sim 2$ for $H_2^{13}CO$, indicative of spin evolution in this formaldehyde isotopomer. As a consequence, we have run water models both for the case of the 'canonical' H_2-ratio (3:1) and for the case, in which *all* hydrogen is assumed to be in the para-form. Spanning this extreme range we always put also the $o:p$-ratio of H_2O equal to that of H_2.

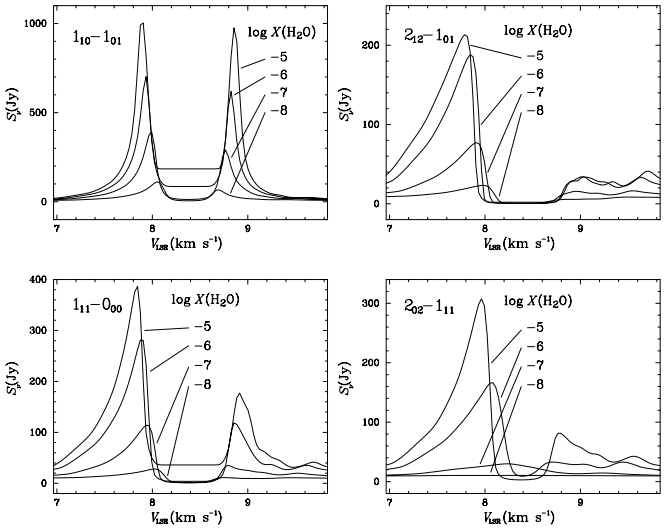

Fig. 8. Predicted low-J ortho- and para-water lines from B 335 as seen with FIRST (space borne 3 m telescope), for $o:p = 3{:}1$ and $X(H_2O) = 10^{-8}$ to 10^{-5}. Flux densities are expressed in Jansky

3.4. Prediction of H_2O line spectra: ODIN observations

For the H_2O calculations, the model cloud consisted of 18 shells. With the density distribution according to the Shu model, some of the water transitions have very high opacities and interact with the gas also at very large radii, where the density is low. The real B 335 cloud is, however, not infinite and we have chosen to cut off our model cloud at the radius of the CS models, viz. at $4.6\,10^{17}$ cm ($2'$ at 250 pc). This corresponds approximately to the extent of the *visual* globule B 335 and may seem somewhat arbitrary. However, since the velocity field outside the infall radius is zero, this choice of cut-off should affect only the depth of the central absorption dip, but not the position and shape of the diagnostic infall peaks and high velocity wings.

In Fig. 7, we present, for different H_2O abundances, the predicted ($1_{10} - 1_{01}$) line of ortho-water at 557 GHz for future observation with the 1.1 m telescope aboard ODIN, a Swedish-International (Canada, Finland and France) satellite for aeronomy and astronomy. The spectrometers aboard this space platform will permit a highest spectral resolution of 0.1 MHz (0.05 km s^{-1} at 557 GHz), so that the line profile is expected to become well resolved. $o:p$ was assumed to be equal to 3. We note that the spectra of this ground state line will depend strongly on this ratio, not only because the ortho-H_2O abundance is dependent on this ratio, but also because, at the actual temperatures, the rate for collisions with para-H_2 for this transition is about 25 times lower than the corresponding rate for collisions with ortho-H_2. Provided that the overall water abundance is higher than about 10^{-7}, this transition should become detectable with ODIN within reasonable integration times. Not totally unexpected, at low H_2O-abundance the 557 GHz line profile is not unlike that of the CS (2-1) and (3-2) lines (see Fig. 7 for $X(H_2O) = 10^{-8}$). With higher abundance the optical depth in the envelope increases and the central absorption dip of the profile becomes flat-bottomed, and remains so out to velocities where the outer parts (envelope) effectively cease to absorb. Only at this point does it become possible to see emission from the central regions. The H_2O emission peaks probe more central regions than do the CS peaks, implying that the separation between the peaks becomes larger. This peak separation increases with increasing water abundance, but its value will be dependent on the telescope beam, as will the apparent intensity ratio of the blue and red peaks (Fig. 7). Since the emission from the infall region is centrally condensed, the envelope contributes progressively more to the total line as the H_2O abundance is increased (cf. also Sect. 3.2).

3.5. Prediction of H_2O line spectra: FIRST observations

In order to make full use of the diagnostic power of the H_2O lines it would be necessary to study several transitions simultaneously. The future FIRST (Far Infrared and Submillimetre Space Telescope, a project of the European Space Agency; see: esa SI(93)6, Sept. 1993) will most probably provide both the required sensitivity and spatial/spectral resolution over a wide frequency band. Our simulation of a FIRST observation is shown in Fig. 8, where we present H_2O line profiles towards B 335 for $X(H_2O) = 10^{-8}$ to 10^{-5} and $o:p$ of H_2 and H_2O equal to 3:1. For the FIRST beam we assumed a telescope size of 3 m. Similarly, in Fig. 9 the para-H_2O lines of the previous figure are shown assuming that the molecules are all in their para states [the profiles for $X(H_2O) = 10^{-5}$ are not shown, since it is not certain that these computations actually converged].

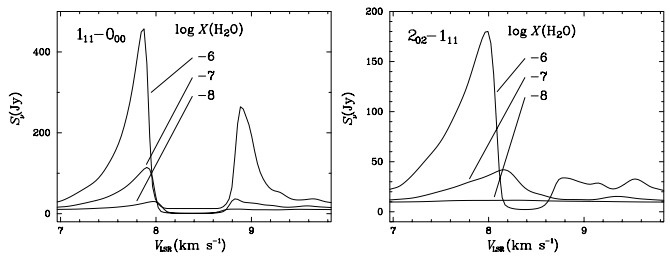

Fig. 9. Same as Fig. 8, but for the case of *all* H_2O and H_2 being in their para states

4. Discussion

4.1. CS line wings: infall or outflow?

The predicted CS profiles from the Shu infall model compare quite well with those observed, if one disregards the excess emission observed in the line wings. Z93 argued that these wings are not formed in the infalling gas but should be attributed to the bipolar molecular outflow. From high resolution CO observations, Hirano et al. (1992) have determined (in LTE) the momentum transfer rate to the 'CO outflow' gas on the spatial scale of 30″, viz. $\dot{P}_{\rm CO} = 6\,10^{-5}\,{\rm M}_\odot\,{\rm km\,s^{-1}\,yr^{-1}}$ (which is a lower limit given that the geometry is non-spherical). Using the same standard techniques and applying the CS abundance of our best fit CS model for the mass estimates in the blue and red wings, we obtain $\dot{P}_{\rm CS} = 2\,10^{-5}\,{\rm M}_\odot\,{\rm km\,s^{-1}\,yr^{-1}}$ for *both* CS (2-1) *and* (3-2). Accounting for the difference in mean molecular weight (Hirano et al. used 1.36, whereas we assumed 2.4), this value is smaller by a factor of five than that estimated from the CO data. In addition, the CS (3-2) blue and red wing emission is not extended along the outflow, but is observed to be compact ($< 30''$; Menten et al. 1989). Given also the force mismatch, one feels, perhaps, not convinced that the origin of the CS wings is to be identified entirely with the B 335 outflow.

A different suggestion for the origin of the CS line wings would be turbulent interaction of the infalling gas, e.g., with the outflow or with magnetic fields. For the sake of profile fitting we mimicked that by varying the radial dependence of the microturbulent velocity, $\xi_{\rm turb}$. Since such is incompatible with the solution of the Shu infall, we approximated the structure variables by power laws (cf. Fig. 1), viz. $n \propto r^{-3/2}$ and $v \propto r^{-1/2}$, corresponding to Bondi accretion at late times of the collapse (see: Tohline 1982). Good fits to the observed line wings (and cores) required the microturbulence being constant = 0.12 km s^{-1}, from $r/r_{\rm max} = 1.0$ to 0.05 ($r_{\rm max} = 4.6\,10^{17}$ cm), and, from there on, increasing linearly to 1.5 km s^{-1} towards the centre. For the comparison with the observations, the velocity offsets applied to the computed CS lines, were the same as previously (Sect. 3.1), except for the (3-2) line which was shifted by +0.10 km s^{-1}. The CS profiles from this model are shown together with the observations by Z93 in the right hand panels of Fig. 4. If $\xi_{\rm turb}$ can be physically identified with the Alfvén speed in the cloud plasma, magnetic field strengths of ~ 3 mG at the radius of 3 AU would be indicated on the basis of the power law model, obviously not in conflict with the upper limit of a few mG on the 10^4 AU scale observationally determined for B 335 by Rydbeck et al. (1980). However, in this case, we would expect the value of λ not to exceed $\frac{1}{6}$, where $\xi_{\rm turb} \propto n^\lambda$ and $\lambda = \frac{1}{2}(2\kappa - 1)$ for $B \propto n^\kappa$ and $\frac{1}{3} \leq \kappa \leq \frac{2}{3}$ (Mouschovias 1976), and, hence, other sources of turbulence would appear more likely.

4.2. H_2O rotational line emission

Our model with constant water abundance throughout the cloud may not be realistic. In particular, water may be frozen out onto the dust grains. If the water has had time to freeze out, one would not expect any appreciable amounts of water vapour to be found in other than in the innermost part, i.e. around the central protostellar source, where the models by Ceccarelli et al. (1996) may apply. On the other hand, the freeze-out time for water can be relatively long. Brown et al. (1988) have calculated the formation of water and its deposition on grains for cold collapsing clouds. According to this model, the water abundance reaches a maximum of $X({\rm H_2O}) = 10^{-5}$ at an age of the cloud slightly less than 10^6 yr. Beyond this peak value, the freeze-out is efficient and at an age of $> 10^6$ yr, the water vapour abundance will rapidly drop to $X({\rm H_2O}) < 10^{-12}$. Consequently, if large scale freeze-out has already occurred in B 335, the gaseous water abundance could be much less than even in our most 'pessimistic' model. In this case, we would expect any H_2O lines to originate only in the inner core region, where temperatures and densities are high enough to evaporate the water ice.

With respect to 'purely thermal' infall lines, the H_2O profiles might become contaminated by emission from shocked gas, either in the infalling gas or in the outflow. Shocks are expected to be efficient producers of water vapour, and are effectively cooled through H_2O lines (see: e.g., Neufeld & Hollenbach 1994). Infall profiles should be easily distinguishable from those generated by shocks, though, since the latter are expected to be considerably broader, by at least several km s^{-1}.

4.3. CO and H_2O cooling rates

For our best fit CS model (Shu-type infall) and for an abundance of $X(^{12}{\rm CO}) = 10^{-4}$ we obtain the cooling rate from the ^{12}CO lines to be $4.6\,10^{30}$ erg s^{-1}. Similarly, for the isotopic abundances determined in Sect. 3.2, viz. $X(^{13}{\rm CO}) = 5\,10^{-6}$ and $X({\rm C^{18}O}) = 5\,10^{-7}$, we find the cooling rate in the ^{13}CO lines as $1.4\,10^{30}$ erg s^{-1} and in the C^{18}O lines as $3.6\,10^{29}$ erg s^{-1}. The total cooling provided by *all* isotopic CO in the infalling gas proceeds, therefore, at the rate of $6.4\,10^{30}$ erg s^{-1} ($1.7\,10^{-3}\,{\rm L}_\odot$). All the lower CO transitions, up to $J \sim 8$, are found to contribute appreciably to the cooling. The total cooling rate due to the water lines, as a function of the water abundance and for both $o:p$ = 3:1 and 0:1, is shown in Table 1. In contrast to CO, the ground state transitions, viz. (1_{10}-1_{01}) and (1_{11}-0_{00}), are responsible for the major part of the cooling by ortho-H_2O and by para-H_2O respectively. From the table it is evident that for the present model of B 335 cooling through the CO lines is

Table 1. H_2O cooling rates (in erg s^{-1}) for B 335: inside-out collapse at the rate $\dot{M} = 2.9\,10^{-6}\,M_\odot\,yr^{-1}$

	$o:p = 3:1$			$o:p = 0:1$
X_{H_2O}	$L(o\text{-}H_2O)$	$L(p\text{-}H_2O)$	$L(H_2O)$	$L(p\text{-}H_2O)$
10^{-5}	$1.9\,10^{30}$	$1.7\,10^{30}$	$3.6\,10^{30}$	–
10^{-6}	$7.1\,10^{29}$	$3.3\,10^{29}$	$1.0\,10^{30}$	$1.1\,10^{30}$
10^{-7}	$2.0\,10^{29}$	$8.9\,10^{28}$	$2.9\,10^{29}$	$9.6\,10^{28}$
10^{-8}	$6.2\,10^{28}$	$2.5\,10^{28}$	$8.7\,10^{28}$	$3.3\,10^{28}$

more important than water cooling. The *precise* cooling rates will depend on details of the models but, recalling that B 335 is representative of cold dense cores, we are led to suggest that there is little reason to believe water to be the dominant coolant of *low*-mass protostellar infall.

4.4. Limitations of the presented model and future work

Apparently, the Shu infall model is fairly successful in reproducing the observed CS lines. This might, perhaps, be somewhat surprising, since this model appears rather simplistic compared to the likely complexity of reality. For instance, rotation and non-spherical geometry were not considered.

Observations in the dust continuum show that the structure of B 335 is elongated on the spatial scales of our models (e.g. Chandler & Sargent 1993). However, the rotation of B 335 is observed to be low (Frerking et al. 1987) and the 'centrifugal radius' is as small as about 3 AU (Z93). Rotation can be expected, therefore, to have negligible effects on the line profiles compared to radial infall on larger spatial scales. The correctness of this assertion was recently demonstrated by Zhou (1995), who modeled the CS lines from B 335 taking rotation explicitly into account and found the line profiles towards the center position unaltered.

The assumption of a smooth density distribution may not be correct. There is evidence that, for instance, the CCS emission in B 335 has a clumpy distribution (Velusamy et al. 1995). An inhomogenous density structure should have effects on the line formation not predicted by our model. However, in the clumps, the (1-0) transitions of the isotopic CO would still be thermalized and the emission could be, therefore, much less sensitive to density than the CS emission. There is the risk, then, that a smooth model of an inhomogeneous cloud will underestimate the level of CS emission compared to that in the isotopic CO lines. This would have the effect that a model based on a best fit to observed CS spectra would predict too high intensities of the CO lines and could be yet another explanation for the necessity of applying the scaling factor < 1 to the observed ^{13}CO and $C^{18}O$ lines.

In the present formulation of our MCM code, complete redistribution in frequency of the photons (equal emission and absorption profile functions) has been implicitly assumed. The possibility of implementing an explicit and (perhaps) more realistic photon scattering function should be investigated in the future. Further, the model presented in this work is not fully self consistent, in the sense that the temperature structure and the chemistry have to be specified from the outset. Ideally, the model should include the energy transfer and time dependent chemistry coupled to the dynamical equations in all three spatial dimensions. Such general approach is, however, still far beyond the capability of presently available computing tools, but should be seen as a goal of future work.

5. Conclusions

In short, we conclude the following:

1. We have developed a Monte Carlo method for radiative transfer at very high optical depths ($\tau \gg 10^4$) by adopting Rybicki's 'core saturation method' for spectral resonance lines.
2. As an example, we have applied this code to the Shu-type infall model of the protostellar source B 335 for the computation of H_2O line profiles for a variety of H_2O abundances and ortho-to-para ratios. These model computations are meant to eventually aid the interpretation of H_2O line observations with space borne facilities, such as ODIN and FIRST.
3. The B 335 model was selected on the basis of the best fit (in a χ^2 sense) to existing CS observations, which have previously been shown to be well explained by spherical Shu-type infall (Zhou et al. 1993, 1994; Choi et al. 1995). Permitting the microturbulence to increase towards the centre results in good fits of the observed CS line *wings* as well.
4. From the Shu-type model and the interferometric observations of the ^{13}CO and $C^{18}O$ (1-0) line profiles (Chandler & Sargent 1993) we estimate the isotopic CO abundances and compute the cooling rates of all CO isotopomers for B 335. From comparison with the cooling rates of H_2O we conclude that H_2O is unlikely to dominate the cooling of low-mass protostellar infall.

Acknowledgements. This work is partially in preparation of the ODIN mission and the support by the Swedish National Space Board is acknowledged. We wish to thank B. Gustafsson, H. Olofsson, G. Olofsson and R. Svensson for stimulating discussions and the anonymous referee for valuable comments.

Appendix A: the Monte Carlo method of radiative transfer

For clarity, the equations below are presented for a two energy level molecule, but the generalization to the multilevel case of the code is quite straightforward.

Model photons with a weight W in proportion to the number of real photons emitted by the source are sent out in random directions and at random frequencies. To save time the model photons represent every transition simultaneously, and thus they have a separate weight for each transition. In addition to photons from the molecular gas, photons which represent background radiation, dust radiation and radiation from a central black body (star) can also be emitted. The cloud is composed of a series

of concentric spherical shells, each having its own values of the physical parameters such as density, temperature, etc. The model photons are followed across the cloud, causing excitations and de-excitations along their paths, which affect the level populations in the different shells. The total number of induced de-excitations, $u \rightarrow l$, as a photon of weight W travels from $x = 0$ to $x = s_1$ is given by

$$N_{ul} = \frac{h\nu}{4\pi}\,\phi_\nu\,n_{u,m}\,B_{ul}\int_0^{s_1} W(x)\,dx \quad , \tag{A1}$$

where m is the index denoting the shell and the other symbols have their usual meaning. The total number of molecules in the upper energy state in shell m is $n_{u,m}V_m$, where V_m is the volume of the shell. With $W = W_0 e^{-\tau}$, we can write the number $S_{ul,m}$ of radiative de-excitations *per molecule in the upper state* in shell m as

$$S_{ul,m} = \frac{N_{ul}}{n_{u,m}V_m} = \frac{h\nu}{4\pi}\,\phi_\nu\,B_{ul}\,\frac{s_1 W_0}{V_m \tau_1}\left(1 - e^{-\tau_1}\right) \quad , \tag{A2}$$

where τ_1 is the optical depth along the distance s_1. The optical depth is calculated as

$$\tau_1 = \frac{h\nu}{4\pi}\phi_\nu\,(n_l B_{lu} - n_u B_{ul})\,s_1 \quad . \tag{A3}$$

$S_{ul,m}$ is accumulated in sums $\sum S_{ul,m}$. When all the model photons have been emitted, new level populations are calculated from the equation of statistical equilibrium,

$$\begin{aligned} &n_l\left(\tfrac{B_{lu}}{4\pi}\int\int I_\nu\,\phi_\nu\,d\nu\,d\omega + C_{lu}\right) = \\ &n_u\left(A_{ul} + \tfrac{B_{ul}}{4\pi}\int\int I_\nu\,\phi_\nu\,d\nu\,d\omega + C_{ul}\right) \quad , \end{aligned} \tag{A4}$$

which in the Monte-Carlo formulation is written as

$$n_l\left(\frac{g_u}{g_l}\sum S_{ul,m} + C_{lu}\right) = n_u\left(A_{ul} + \sum S_{ul,m} + C_{ul}\right) . \tag{A5}$$

After adjustment of the level populations, new model photons are sent out, and the process is repeated. In order to reduce the random noise, the $\sum S_{ul,m}$ counters are not emptied every iteration, and $\sum S_{ul,m}$ is then replaced by $\sum S_{ul,m}/N_{\rm iter}$ in the statistical equlibrium equation. The iteration is continued either for a fixed number of iterations, or until some pre-specified criterion for convergence is fulfilled.

Appendix B: Monte Carlo method with core saturation

B.1. Implementation of the core saturation method

The core saturation method is only applied to photons emitted by the molecular gas (i.e not to those from the dust or the background radiation). When a model photon is emitted, the optical depth to the nearest boundary is calculated, and it is decided, whether the photon is in the core of the line. As the distinction between core and wing is not precise, we follow Flannery et al. (1980) by introducing an exponentially tapered weighting function, $\mathscr{T}$, which tends to unity in the wing and to zero in the core, but also allows intermediate cases, viz.

$$\mathscr{T} = \begin{cases} e^{1-\tau/\gamma} & \text{if } \tau/\gamma > 1 \\ 1 & \text{if } \tau/\gamma < 1 \end{cases} . \tag{B1}$$

γ is the customary adjustable parameter, which roughly represents the optical depth separating the core and the wing. A smaller γ will result in faster convergence, but if it is made too small, the code will not converge. Note that even though the core photons are eliminated in the calculations, we must continue to follow every model photon, as each model photon represents all the transitions simultaneously.

The ratio of photons in the wing, n_w, to the total number of photons emitted by the gas is given by

$$n_w = \frac{\sum \mathscr{T}}{n_{\rm gas\ phot}} \quad . \tag{B2}$$

In the core saturation method, the core photons are eliminated from the statistical equilibrium equation, implicitly making use of the approximation $I_\nu = B_\nu(T_{\rm ex})$ in the core. This leads to much faster convergence and is possible, because these photons contribute so little to the energy transport. The statistical equilibrium equation is modified to

$$\begin{aligned} &n_l\left(\tfrac{B_{lu}}{4\pi}\int\int I_\nu\,\phi_\nu\,\mathscr{T}\,d\nu\,d\omega + C_{lu}\right) = \\ &n_u\left(A_{ul}n_w + \tfrac{B_{ul}}{4\pi}\int\int I_\nu\,\phi_\nu\,\mathscr{T}\,d\nu\,d\omega + C_{ul}\right) \end{aligned} \tag{B3}$$

and, in Monte-Carlo formulation, one arrives at

$$\begin{aligned} &n_l\left(\frac{g_u}{g_l}\sum S_{ul,m}\mathscr{T} + C_{lu}\right) = \\ &n_u\left(A_{ul}n_w + \sum S_{ul,m}\mathscr{T} + C_{ul}\right) \quad . \end{aligned} \tag{B4}$$

For simplicity, the core saturation procedure is only executed in the shell where the photon in question was created, since the core photons will in any case never travel far.

B.2. Correcting the core saturation for lost photons

The core saturation method simply neglects the energy transport in the core. This will cause an error, which becomes larger as γ is decreased, i.e. as the frequency space defining the core grows larger. We introduce a procedure, where a correction term, $\mathscr{C}_{ul,m}$, is added to the statistical equilibrium equation. $\mathscr{C}_{ul,m}$ represents the difference between the correct number of radiative de-excitations per molecule in the upper state, $\sum S_{ul,m}$, and the implicit aproximation in the core saturation method, $B_\nu B_{ul}$. The equation of statistical equilibrium with the correction term included reads

$$\begin{aligned} &n_l\left[\frac{g_u}{g_l}\left(\sum S_{ul,m}\mathscr{T} + \mathscr{C}_{ul,m}\right) + C_{lu}\right] = \\ &n_u\left(A_{ul}n_w + \sum S_{ul,m}\mathscr{T} + \mathscr{C}_{ul,m} + C_{ul}\right) \quad . \end{aligned} \tag{B5}$$

Every photon contributes a certain amount $S_{ul,m}$ to the de-excitations. For a certain gas photon in the core, this is aproximated by $B_\nu B_{ul} W_0/\sum W_0$, where the subscript 0 refers to the initial value of the photon weight. Using the excitation temperatures from the previous iteration, $\mathscr{C}_{ul,m}$ can then be calculated

as

$$\mathscr{C}_{ul,m} = \sum_{\text{gas phot}} \left[S_{ul,m} - B_\nu(T_{\text{ex}}) B_{ul} W_0 / \sum W_0\right] \left(1 - \mathscr{T}\right) \quad . \quad \text{(B6)}$$

The total weight, $\sum W_0$, of the model photons emitted in shell m is equal to the total number of real photons emitted, $n_u A_{ul} V_m$. From Eqs. (A2) and (A3) and using the relations

$$B_\nu(T_{\text{ex}}) = \frac{2h\nu^3}{c^2} \frac{1}{\frac{g_u n_l}{g_l n_u} - 1} \quad , \quad A_{ul} = \frac{2h\nu^3}{c^2} B_{ul}$$

and $B_{ul} = \frac{g_l}{g_u} B_{lu}$

one finds

$$S_{ul,m} = \frac{W_0 (1 - e^{-\tau})}{V_m \left(n_l \frac{g_u}{g_l} - n_u\right)} \quad \text{(B7)}$$

and

$$B_\nu B_{ul} W_0 / \sum W_0 = \frac{W_0}{V_m \left(n_l \frac{g_u}{g_l} - n_u\right)} \quad \text{(B8)}$$

so that one finally can write

$$\mathscr{C}_{ul,m} = \sum_{\text{gas phot}} - \frac{S_{ul,m}}{e^\tau - 1} \left(1 - \mathscr{T}\right) \quad . \quad \text{(B9)}$$

which is the expression actually used in the code.

References

Bergman P., 1985, Numerisk simulering av strålningstransport i klumpade och inhomogena molekylmoln, Onsala Space Observatory Report

Bernes C., 1979, A&A 73, 67

Brown P.D., Charnley S.B., Millar T.J., 1988, MNRAS 231, 409

Cabrit S., Goldsmith P.F., Snell R.L., 1988, ApJ 334, 196

Ceccarelli C., Hollenbach D.J., Tielens A.G.G.M., 1996, ApJ 471, 400

Chakerian C., Tipping R.H., 1983, Journ. of Mol. Spec. 99, 431

Chandler C.J., Sargent A.I., 1993, ApJ 414, L 29

Chandler C.J., Gear W.K., Sandell G., et al., 1990, MNRAS 243, 330

Chandra S., Varshalovich D.A., Kegel W.H., 1984, A&AS 55, 51

Choi M., Evans N.J., II, Gregersen E.M., Wang Y., 1995, ApJ 448, 742

Flannery B.P., Rybicki G.B., Sarazin C.L., 1980, ApJS 44, 539

Flower D.R., Watt G.D., 1984, MNRAS 209, 25

Flower D.R., Launay J.M., 1985, MNRAS 214, 271

Frerking M.A., Langer W.D., Wilson R.W., 1987, ApJ 313, 320

Green S., Chapman S., 1978, ApJS 37, 169

Gregersen E.M., Evans II N.J., Zhou S., Choi M., 1997, ApJ 484, 256

Hirano N., Kameya O., Nakayama M., Takakubo K., 1988, ApJ 327, L 69

Hirano N., Kameya O., Kasuga T., Umemoto T., 1992, ApJ 390, L 85

Hollenbach D., Ceccarelli C., Neufeld D.A., Tielens A.G.G.M, 1995 in: Airborne Astronomy, Haas M.R., Davidson J.A., Erickson E.F. (eds.), ASP Conf. Ser. Vol. 73, p. 243

Juvela M., 1997, A&A 322, 943

Keene J., Davidson J.A., Harper D.A., et al., 1983 ApJ 274, L 43

Langer W.D., Frerking M.A., Wilson R.W., 1986, ApJ 306, L 29

Mathis J.S., Mezger P.G., Panagia N., 1983, A&A 128, 212

Menten K.M., Harju J., Olano C.A., Walmsley C.M., 1989, A&A 223, 258

Mihalas D., 1978, Stellar Atmospheres, 2nd ed., San Francisco, Freeman

Minh Y.C., Dickens J.E., Irvine W.M., McGonagle D., 1995, A&A 298, 213

Moriarty-Schieven G.H., Snell R.L., 1989, ApJ 338, 952

Mouschovias T.Ch., 1976, ApJ 207, 141

Neufeld D.A., Hollenbach D.J., 1994, ApJ 428, 170

Phillips T.R., Maluendes S., Green S., 1996, ApJS 107, 467

Rybicki G.B., 1972, in: Line Formation in the Presence of Magnetic Fields, R.G. Athay, L.L. House, G. Newkirk, Jr. (eds.), Boulder, High Altitude Observatory, p. 145

Rydbeck O.E.H., Irvine W.M., Hjalmarson Å., et al., 1980, ApJ 235, L 171

Shu F.H., 1977, ApJ 214, 488

Tohline J.E., 1982, Fund. Cosm. Phys. 8, 1

Turner B.E., Chan K.-W., Green S., Lubowich D.A., 1992, ApJ 399, 114

Velusamy T., Kuiper T.B.H., Langer W.D., 1995, ApJ 451, L 75

Willacy K., Williams D.A., Minh Y.C., 1993, MNRAS 263, L 40

Zhou S., 1995, ApJ 442, 685

Zhou S., Evans II N.J., Butner H.M., 1990, ApJ 363, 168 (Z90)

Zhou S., Evans II N.J., Kömpe C., Walmsley C.M., 1993, ApJ 404, 232 (Z93)

Zhou S., Evans II N.J., Kömpe C., Walmsley C.M., 1994, ApJ 421, 854 (Z94)

This article was processed by the author using Springer-Verlag LaTeX A&A style file *L-AA* version 3.